AIAA 2013-2079

Experimental Study of Flight Effects on Slightly Underexpanded Supersonic Jets

Benoît André *, Thomas Castelain † and Christophe Bailly ‡

Laboratoire de Mécanique des Fluides et d'Acoustique, UMR CNRS 5509 & Ecole Centrale de Lyon, 36 Avenue Guy de Collongue, 69134 Ecully Cedex, France

The flight effects on the turbulence properties and the shock-cell system of slightly underexpanded supersonic jets are studied experimentally. To do so, particle image velocimetry, schlieren visualizations and pressure measurements are used in a dual-stream geometry, whose outer flow simulates flight up to a Mach number of 0.4. The study of turbulence includes the evolution under simulated flight of the momentum thickness of the mixing layer, of integral time and length scales, and of turbulence levels. The analysis of the shock-cell structure comprises an evaluation of flight effects on the length of the pattern and on the length and strength of the shock cells. Several discrepancies with other studies are pinpointed and discussed.

Nomenclature

Latin characters

D	Nozzle diameter
D_j	Perfectly expanded jet diameter
L_s	Shock-cell length
L_s^{f}	Shock-cell length in flight conditions, as opposed to L_s^{g}
L_s^{g}	Shock-cell length in static conditions, as opposed to L_s^{f}
$L_{ii}^{(k)}$	Integral length scale of turbulence, see Eq. (3)
M_f	Flight Mach number
M_j	Perfectly expanded jet Mach number
P_s	Static pressure
$P_{\min}$	Minimum static pressure inside a shock cell
$P_{\max}$	Maximum static pressure inside a shock cell
P_{amb}	Ambient pressure
R_{ij}	Correlation coefficient of u, see Eq. (2)
T_{cii}	Integral time scale of turbulence in the convected frame, see Eq. (4)
u	Instantaneous velocity
U_j	Mean velocity in the supersonic jet
U_f	Flight velocity
x	Longitudinal coordinate
y	Transverse coordinate

Greek characters

β	Shock parameter, $(M_j^2 - 1)^{1/2}$
δ_θ	Shear layer momentum thickness
ΔU	Mean velocity difference across the jet shear layer
σ	Root-mean-square value of the velocity fluctuations

*Postdoctoral fellow, Laboratoire de Mécanique des Fluides et d'Acoustique, Ecole Centrale de Lyon.
†Assistant professor, Université Lyon 1, 43 Boulevard du 11 Novembre 1918, 69622 Villeurbanne Cedex.
‡Professor, Ecole Centrale de Lyon & Institut Universitaire de France, Senior AIAA Member.

Vectors

$\boldsymbol{x}$	Reference point of calculation
$\boldsymbol{\xi}$	Separation vector

Subscripts and superscripts

i, j, k	Variable numbers within (1,2)

Operators

$\overline{\cdot}$	Ensemble average of $\cdot$
$\cdot'$	Fluctuating component of $\cdot$

I. Introduction

Flight effects on jet noise have been extensively studied as of the 1970s. There is indeed an interest in understanding the changes brought about by the external flow coming from the aircraft flight on the structure of the jet exhausted by the turbofan engines and on the emitted mixing noise. The goal is usually to tackle the issue of community noise. Most of the early studies combined theoretical developments and acoustic experiments,[1,2] but some also presented aerodynamical measurements. For instance, Morris[3] investigated flight effects on subsonic and fully expanded supersonic jets by means of a laser Doppler velocimeter. His results were then used by Tanna & Morris[4] as inputs into a theory of flight effects on mixing noise. Larson *et al.*[5] also addressed many aspects of the turbulence of a subsonic jet with external stream from single- and two-probe hot wire measurements, like mixing layer growth, turbulence level, convection velocity, or integral time and length scales. They subsequently used these data to predict the relative velocity exponent, summarizing the overall mixing noise reduction in flight.

The commercial aircraft powered by turbofan engines exhaust slightly underexpanded supersonic jets at cruise, characterized by the presence of a shock-cell pattern in the jet plume.[6,7] The interaction in the jet mixing layer between the turbulence and the shock-cell system is responsible for the so-called shock-associated noise component of jet noise, which is in addition to the turbulent mixing noise. Shock-associated noise is made up of two distinct parts : a tonal one, referred to as screech,[8,9] and a broadband one[10,11] (it seems however that only the broadband component is emitted in the practical, full-scale problem).

The use of composite materials, inducing lower sound transmission losses than classical metallic structures, in the fuselage of the next-generation aircraft, has raised concerns about the noise levels in the cabin. Hence, there is currently a renewed interest for studying the behavior of shock-associated noise in flight. A short overview of relevant past works is presented now. Bryce & Pinker[12] showed that the shock cells of underexpanded jets lengthen with secondary flow. Sarohia[13] presented shadowgrams of supersonic jets in flight beside acoustic measurements, with a study of the effect of the initial conditions on the jet. Norum & Shearin[14–16] performed extensive acoustic measurements as well as static pressure surveys to determine the flight effects on the shock-cell structure and the shock-associated noise, up to a flight Mach number M_f of 0.4. Their study was extended to higher values of M_f by Norum & Brown.[17] In these works, no account of turbulence was given. More recently, Rask *et al.*[18] measured flow and acoustic pressure and applied particle image velocimetry (PIV) to a dual-stream configuration with a chevron nozzle to understand the influence of this device on supersonic jet noise in flight. From their PIV results, they presented turbulent kinetic energy profiles. Further data on turbulence in a shock-containing jet under flight conditions will help modeling supersonic jet noise.

The effects of flight on the aerodynamical development of slightly underexpanded jets are investigated in this paper. Firstly, the experimental methods employed are presented. Secondly, the flight effects on the turbulence and the shock-cell structure are deduced from PIV results, pressure measurements and schlieren visualizations.

II. Experimental methods

The dual-stream facility employed for the present study has already been described in reference.[19] Only a brief account is given here.

The supersonic jet flow originates from a continuously operating compressor mounted upstream of an air drier. Two contoured convergent nozzles are used. One is a round nozzle of diameter 38.25 mm. It will be referred to as the plain nozzle in the following. The second one has a diameter of 38.7 mm and has shallow notches cut into its lip. It has been shown that this nozzle non-intrusively suppresses screech.[20] In order to better simulate the conditions arising in air transport, most of the results have been obtained with the screech-suppressing nozzle, in particular the entire turbulence data from the PIV. However, the plain nozzle was mounted for the static pressure measurements. As explained in section III.A.4, the conclusions reached are believed to also apply in a jet without screech.

The reservoir temperature T_t is measured upstream of the exit. Here, the jets are unheated and $T_t \approx 30°$. The nozzle pressure ratio (NPR), defined as the ratio between jet stagnation pressure and ambient pressure, is set by measuring the wall static pressure fifteen nozzle diameters upstream of the exit. In the following, results for jets of ideally expanded Mach number $M_j = 1.10$ and 1.15 are presented, corresponding to NPR = 2.14 and 2.27, respectively. The shock parameter $\beta = \sqrt{M_j^2 - 1}$ will also be used.

The subsonic jet is generated by a fan system and exhausts through a 200 mm-diameter contoured convergent nozzle. Well upstream of the exit, the supersonic duct penetrates into the subsonic flow. In the final section before the exit, both ducts are cylindrical and coaxial and the two jets have the same exit plane. The adequacy of the ratio between the supersonic and the subsonic jet diameter for flight simulation has been checked in reference.[19] The flight Mach number, written M_f, can be varied from 0 to 0.4 approximately. Results are obtained for $M_f = 0$ (or 0.05), 0.22 and 0.39.

A conventional Z-type schlieren system is used to visualize the flow. It consists of a light-emitting diode as light source, two 203.2 mm-diameter f/8 parabolic mirrors, a straight knife-edge set perpendicular to the flow direction and a high-speed CMOS Phantom V12 camera.

Static pressure measurements have been performed by means of short static probes based on a design by Pinckney.[21] They have an outer diameter of 1.5 mm and a tip to static hole distance smaller than 5 mm. Their compact geometry aims at solving the difficulty of measuring pressure in a flow with high gradients. Such probes have been extensively used for shock-cell structure characterizations, especially in connection with broadband shock-associated noise.[16,22] Some of our results have been compared with static pressure profiles by Norum & Seiner[22] and a good agreement has been found.

Particle image velocimetry (PIV) has also been applied to the jet exhausting from the notched nozzle. Velocity is measured in a plane containing the jet axis and a notch. Illumination is provided by a pulsed double-cavity Nd:YLF Quantronix Darwin Duo laser. The sheet thickness is 1.7 mm ± 0.3 mm. The supersonic jet is seeded with olive oil by means of custom-designed Laskin nozzle generators. The mean particle size is known to be around 1 μm. The subsonic flow is seeded by smoke; the static condition ($M_f = 0$) is replaced by a minimum flight Mach number of 0.05 to ensure seeding of the supersonic jet surroundings. Both seeding devices are mounted far enough upstream of the exit so that the particle concentration in each flow is approximately uniform. Two CMOS Phantom V12 cameras of sensor size 1280×800 pixels^2 are set side by side to double the field of view available. The acquisition frequency is 500 Hz and the magnifying factor for each camera is about 0.05 mm/pixel. The PIV set-up is mounted on a frame which can be translated in the jet direction. For each position, a length of about two jet diameters is viewed by the camera system. An axial extent of 12 D is studied here, meaning that the entire field has been acquired in six parts. For each new location of the frame, calibration of the camera images is performed using a three-dimensional LaVision plate, the jet operating conditions are reset and 2000 particle image pairs are recorded. The vector field calculation is performed by a multigrid FFT-based technique using the LaVison DaVis 7.2 software. In all but the last iteration, the calculation is a two-step process; a 25%-overlap of the interrogation windows is set and no window ponderation is used. For the last iteration, three computational steps are set, as well as a 50%-overlap and a Gaussian window ponderation. The final correlation windows are of size 8×8 pixels^2, leading to a vector density of one every 0.2 mm, or approximately 190 vectors across the supersonic jet diameter.

The behavior of the seeding particles in imperfectly expanded jets was studied in reference[7] from laser Doppler velocimetry (LDV) data. It was concluded that the particles followed accurately the flow in slightly underexpanded jets and even in the presence of a Mach disc. The mean velocity results obtained by PIV have been compared to LDV profiles and a good agreement has been found.

In the following, the supersonic jet diameter will be called D, whatever the nozzle is. The origin of the coordinates is taken at the center of the mounted nozzle. The variable x will denote the longitudinal direction and y the transverse direction.

III. Results

The topics treated in the following are addressed in reference[23] for underexpanded jets without simulated flight. The same analysis is performed here, so that only a brief account of the data reduction procedures is provided.

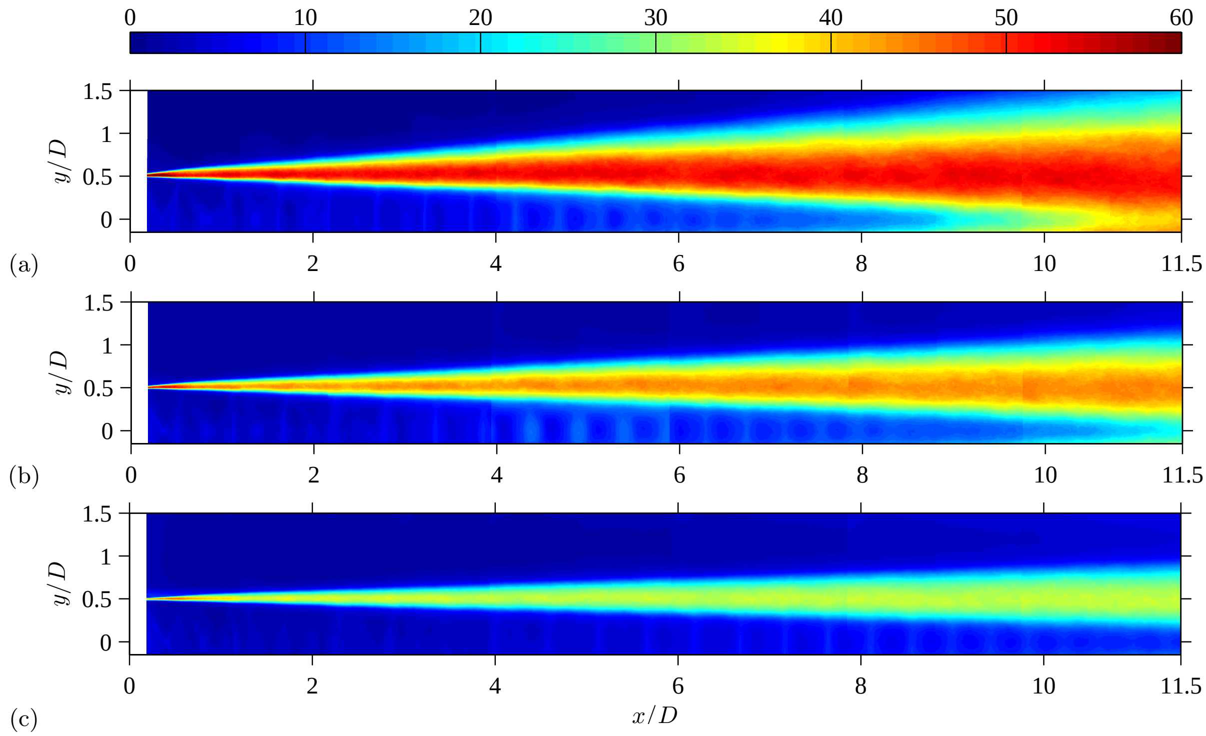

Figure 1. Cartography of σ_1, the root-mean-square longitudinal velocity fluctuations, for $M_j = 1.10$ and (a) $M_f = 0.05$, (b) $M_f = 0.22$ and (c) $M_f = 0.39$ (notched nozzle). All three maps have the same colorbar (in m.s^{-1}).

III..1. Turbulence levels

To begin with, the effect of flight on the turbulence levels in the mixing layer is estimated. Owing to the reduced mean velocity shear when M_f is increased, the absolute fluctuation levels decrease in flight. This can be seen in figure 1, where M_f is increased from $M_f = 0.05$ to 0.39 for $M_j = 1.10$. Turbulence being mainly produced by velocity gradients, the ratios of the root-mean-square velocity components (written σ_i, with $i = 1$ for the axial component and 2 for the radial one) over the velocity difference ΔU between the supersonic jet and the low-speed co-flow are formed to provide indicators of the turbulence levels. Since underexpanded supersonic jets are not uniform, it is not obvious which velocity is to be considered to compute ΔU. A mean velocity, noted U_j, is chosen here, about which the axial velocity oscillates in the shock-cell structure. ΔU is then defined as $U_j - U_f$, with U_f the flight velocity.

The flight effects on the peak turbulence levels in the mixing layer are presented in figure 2 for $M_j = 1.10$ and 1.15. In each plot, the three upper curves show σ_1 while the three lower ones correspond to σ_2. Non-dimensioned by ΔU, the peak fluctuation levels are almost constant with M_f, apart in a region near the nozzle exit.

In the literature, there exists a disagreement on how the absolute fluctuation levels decrease with a secondary flow. Goebel & Dutton[24] measured turbulence properties in the fully developed region of several plane, compressible mixing layers using a two-component laser Doppler velocimeter. They found that $\sigma_1/\Delta U$ remained constant with the relative Mach number of the mixing layer, while $\sigma_2/\Delta U$ decreased. Translated into the present problem, this means that $\sigma_1/\Delta U$ should remain constant while $\sigma_2/\Delta U$ should increase when M_f is increased. Morris[3] obtained a dependence of the fluctuation peak on the flight velocity reading $(1 - U_f/U_j)^{0.7}$ whereas written in this form, the present results lead to a proportionality with $(1 - U_f/U_j)^1$. The exponent 0.7 was also obtained by Larson *et al.*[5]

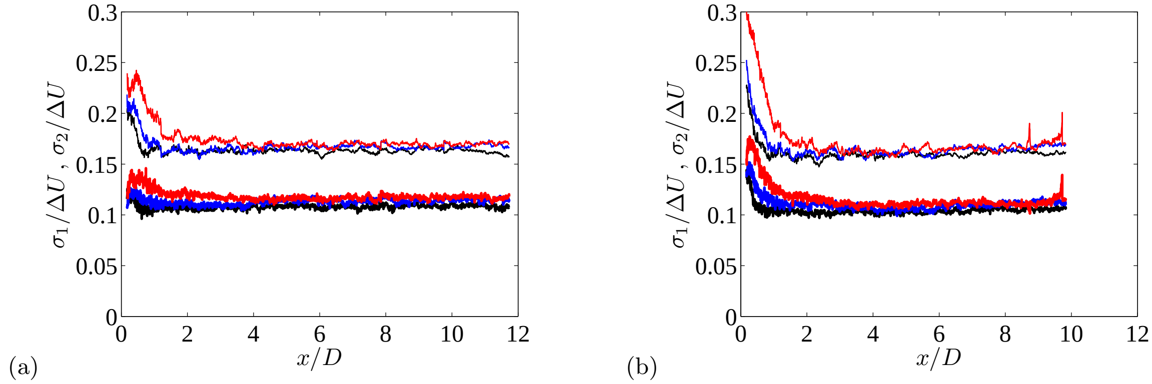

Figure 2. Longitudinal and transverse turbulence levels in the mixing layer. (a) $M_j = 1.10$, (b) $M_j = 1.15$. — $M_f = 0.05$, — $M_f = 0.22$, — $M_f = 0.39$; —, —, — $\sigma_1/\Delta U$, —, —, — $\sigma_2/\Delta U$.

The reason for these discrepancies probably lies in variations in initial conditions. Indeed, Morris[3] hypothesized that his exponent 0.7 should be specific to the experimental facility and believed that if it were not for the persistence of the initial conditions, a linear dependence on the velocity difference should prevail. Similarly, Sarohia & Massier[25] showed by schlieren visualizations and jet noise measurements that the thickness of the boundary layer on the outer side of the primary jet had an influence on the effects of flight. According to them, this external boundary layer leads to a situation where it is as if there were no external flow, at least near the nozzle exit plane. Therefore, turbulence should scale with a velocity greater than ΔU and smaller that the jet velocity on an axial extension depending on the initial boundary layer thickness. It has already been pinpointed that the curves of figure 2 do not collapse in the initial portion of the mixing layer. Choosing U_j as the reference velocity to build the turbulence levels makes the ratios decrease with M_f, meaning that the scaling velocity should be between ΔU and U_j, as proposed by Sarohia & Massier.

In the facility of Ref. 3, the primary jet is placed inside a large wind tunnel. The external boundary can therefore develop on the outer wall of the primary jet nozzle to a significant width. The secondary jet nozzle being, in the present set-up, convergent and of co-planar exit with the primary jet, it is expected that the boundary layer developing on the outer wall of the primary jet nozzle be thinner, leading to a reduced influence of the initial conditions, and the linear dependence of turbulence levels on ΔU as of a short distance downstream of the nozzle exit. The present results confirm therefore the assumption uttered by Morris[3] and recalled above.

A similar discussion about the influence of initial conditions is proposed in section III.A.5 for the effects of flight on the shock-cell structure.

III..2. Momentum thickness

The mixing layer momentum thickness is defined as

$$\delta_\theta = \frac{1}{\left[\overline{u_1}(y_\mathrm{i}) - \overline{u_1}(y_\mathrm{o})\right]^2} \int_{y_\mathrm{i}}^{y_\mathrm{o}} \left[\overline{u_1}(y) - \overline{u_1}(y_\mathrm{o})\right] \left[\overline{u_1}(y_\mathrm{i}) - \overline{u_1}(y)\right] dy \qquad (1)$$

where u_1 is the axial velocity component, y_i and y_o are the mixing layer limits inside and outside the supersonic jet, and the overline denotes the ensemble averaging operator. So as to properly define these boundaries, the fluctuation data obtained by the PIV are used. For each axial station, the radial location of the maximum root-mean-square value of the axial velocity fluctuations is determined. In the high- and low-velocity side of the flow, the fluctuation minima are searched. For each side, the mixing layer boundary is defined as the location where the root-mean-square velocity has decreased to $(1 - \alpha)$ times the difference between the maximum and the minimum of the fluctuations, with α a parameter between 0 and 1. Finally, the integration of equation (1) is performed between these two limits. It has been verified that the value of α had little effect on the estimation of δ_θ and the value $\alpha = 0.9$ is chosen for the subsequent computations.

The evolution of δ_θ along the mixing layer for $M_j = 1.10$ and three values of M_f is shown in figure 3. Firstly, the mixing layer growth is linear for all jets, which is characteristic of fully turbulent mixing layers.[26]

Secondly, the growth rate decreases when M_f is increased. This is a well-known effect of the presence of a secondary stream, coming from the reduced shear across the mixing layer. It was already clearly visible in figure 1. The growth rate decrease or its consequences have already been shown by velocity measurements,[3,5,27] and schlieren visualizations.[13,25] It entails a stretching of the entire flow and in particular a lengthening of the potential core. The numerical values of the growth rates $\mathrm{d}\delta_\theta/\mathrm{d}x$ are given in table 1 for $M_j = 1.10$ and 1.15.

Brown & Roshko[28] and Morris[3] found that the dependence of the mixing layer growth rate on the flight velocity was linear with $r = (1-\lambda)/(1+\lambda)$, where $\lambda = U_f/U_j$. Larson *et al.*[5] rather found a dependence as $r^{0.5}$. Here, it seems that the evolution of the mixing layer growth rate with r be between these two expressions, namely r^n with $n \simeq 0.85$.

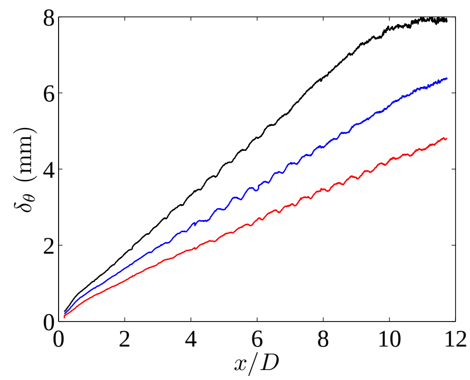

Figure 3. Evolution of δ_θ along the mixing layer with the notched nozzle at $M_j = 1.10$. —— $M_f = 0.05$, —— $M_f = 0.22$, —— $M_f = 0.39$.

	$M_f = 0.05$	$M_f = 0.22$	$M_f = 0.39$
$M_j = 1.10$	0.0199	0.0139	0.0101
$M_j = 1.15$	0.0175	0.0125	0.0091

Table 1. Growth rates of the mixing layer ($\mathrm{d}\delta_\theta/\mathrm{d}x$) as a function of M_j and M_f (notched nozzle).

III..3. Spatial correlations

Spatial correlations are computed from the velocity fields in order to obtain information on the size of the turbulent structures. The coefficient of space-time correlation is written

$$R_{ij}(\boldsymbol{x},\boldsymbol{\xi},\tau) = \frac{\overline{u_i'(\boldsymbol{x},t)\, u_j'(\boldsymbol{x}+\boldsymbol{\xi},t+\tau)}}{\sigma_i(\boldsymbol{x})\,\sigma_j(\boldsymbol{x}+\boldsymbol{\xi})} \tag{2}$$

where the indexes i and j represent the velocity component, $\cdot'$ denotes the fluctuations of $\cdot$, $\boldsymbol{x}$ is the reference point, $\boldsymbol{\xi}$ is the separation vector, t is time and τ is the time delay. Ensemble averages are calculated over the 2000 fields acquired. The indexes 1 and 2 will denote the axial and transverse directions, respectively. In the following, only spatial correlations are computed ($\tau = 0$).

Cross-correlations R_{11} and R_{22} have been estimated while moving the reference point on the horizontal line $y/D_j = 0.5$, with D_j the fully expanded jet diameter, slightly larger than D. This is done to account for the expansion of underexpanded jets. It has been checked however that the precise location of the reference points had a marginal influence on the results.

From R_{ii}, $i \in (1,2)$, it is possible to calculate the correlation length scale of u_i' in the direction k, $k \in (1,2)$, by

$$L_{ii}^{(k)}(\boldsymbol{x}) = \frac{1}{2}\int_{-\infty}^{+\infty} R_{ii}(\boldsymbol{x},\xi_k)\,\mathrm{d}\xi_k \tag{3}$$

where ξ_k is the separation distance in the direction k. In practice, the integration is performed over a finite interval of integration. Here, it is done until the correlation contour of level 0.1 to avoid the low correlation domain which can be noisy; in any case, the integration limit has little influence on the numerical values, and it has to be noted that integral length scales are merely order-of-magnitude estimates.

The evolution of $L_{11}^{(2)}$ along the mixing layer is shown in figure 4 for $M_j = 1.10$ and the three values of M_f. Expectedly, the integral length scale decreases with M_f, since the mixing layer becomes thinner. The ratio of $L_{11}^{(2)}$ with δ_θ is shown in figure 5 and a constant value is reached after a few diameters. This statement remains true for $M_j = 1.15$ and other integral length scales. The proportionality between the integral scales and the mixing layer width is in agreement with the hot wire measurements by Larson *et al.*[5] in an incompressible coaxial jet. It also seems here that the length scales become slightly greater with respect to δ_θ when M_f is increased. To summarize the tendencies obtained, the ratios of the slopes of the scales $L_{ii}^{(j)}$ and of δ_θ are shown in table 2. The length $L_{22}^{(2)}$ is not included since the results are noisier for this scale. It is clear that the ratios increase with M_f, in accordance with the partial results shown in figure 5. This could be an effect of the decreasing compressibility of the mixing layer when M_f becomes larger. Such an interpretation is coherent with the well-known decrease in mixing efficiency induced by increased compressibility.[29,30] Considering the tendencies at fixed M_f, the ratios also rise, although the compressibility *increases*. Hence, compressibility alone cannot explain all the trends. However, another factor may be relevant as well for the evolution with increasing M_j: the degree of underexpansion is changed. Beside compressibility, the strength of the shock-cell pattern could, therefore, also be important in determining the integral length scales.

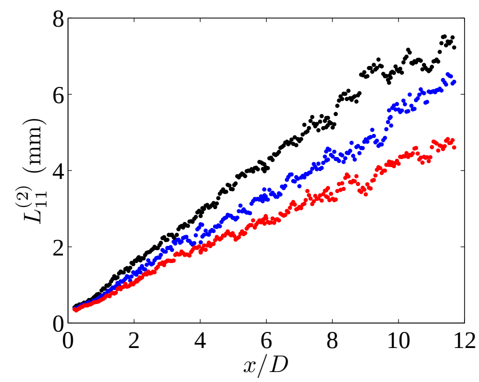

Figure 4. Evolution of $L_{11}^{(2)}$ along the mixing layer, $M_j = 1.10$ (notched nozzle). • $M_f = 0.05$, • $M_f = 0.22$, • $M_f = 0.39$.

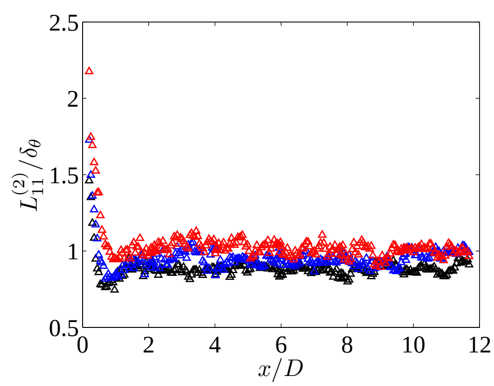

Figure 5. Evolution of $L_{11}^{(2)}/\delta_\theta$ along the mixing layer, $M_j = 1.10$ (notched nozzle). • $M_f = 0.05$, • $M_f = 0.22$, • $M_f = 0.39$.

	$L_{11}^{(1)}/\delta_\theta$			$L_{11}^{(2)}/\delta_\theta$			$L_{22}^{(1)}/\delta_\theta$		
M_f	0.05	0.22	0.39	0.05	0.22	0.39	0.05	0.22	0.39
$M_j = 1.10$	1.76	1.93	1.99	0.83	0.97	0.98	0.56	0.52	0.65
$M_j = 1.15$	1.95	2.28	2.40	0.89	1.01	1.15	0.66	0.78	0.72

Table 2. Ratios of the growth rates of $L_{ii}^{(j)}$ and δ_θ for $M_j = 1.10$ and 1.15, and $M_f = 0.05$, 0.22 and 0.39 (notched nozzle).

III..4. *Integral time scales in the convected frame*

Integral time scales of the turbulence in the convected frame measure the time a structure remains coherent in its motion. It is a very significant information, especially for broadband shock-associated noise (BBSAN). Indeed, an important concept in the BBSAN models proposed by Harper-Bourne & Fisher[10] and Tam[11,31] is the existence of interferences between adjacent sound sources, which arise from the turbulent structures being coherent over several shock cells.

The time scales of the turbulence cannot be deduced directly from the PIV data because of a too low acquisition rate. Following Fleury *et al.*,[32] it can be approximated by

$$T_{cii} \approx \frac{L_{ii}^{(1)}}{\sigma_i} \tag{4}$$

where T_{cii} is the integral time scale in the convected frame for the fluctuating velocity in the direction i. To compute T_{cii}, the maximum fluctuations for each axial station is considered. The effect of flight on T_{c11} is given in figure 6 for $M_j = 1.10$. It is obvious that flight has no effect on the turbulence time scale in the convected frame. The decrease in $L_{11}^{(1)}$ and σ_1 compensate each other to leave T_{c11} unchanged when M_f is increased. This conclusion is also true for $M_j = 1.15$ and T_{c22}. It appears therefore that the two conflicting effects of reduced turbulence levels and reduced integral length scales compensate.

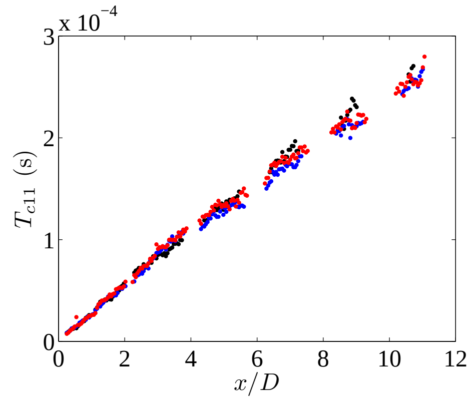

Figure 6. Evolution of T_{c11} with M_f (notched nozzle, $M_j = 1.10$). • $M_f = 0.05$, • $M_f = 0.22$, • $M_f = 0.39$.

III.A. Flight effects on the shock-cell structure

III.A.1. *Effects on the length of the structure*

The entire shock-cell structure of three jets at $M_j = 1.10$ with increasing flight Mach number is shown by the schlieren visualizations in figure 7. It is clear that when M_f is increased, the shock-cell structure is longer, meaning that it includes more shock cells (which is different from the shock-cell lengthening presented later). This phenomenon can be explained by the reduced growth of the mixing layer in flight, emphasized in section III..2. It induces a lengthening of the potential core (particularly visible in figure 1) and the supersonic core, which naturally entails a stretching of the shock-cell pattern. This effect was already stated by Sarohia,[13] and can also be observed on the static pressure measurements by Rask *et al.*[18] and Norum & Brown.[17] In the latter reference, the flight effect is quite spectacular at the maximum M_f value of 0.9, with more than twice as many shock cells as for $M_f = 0$. However, this phenomenon is not very pronounced in the measurements by Norum & Shearin.[16]

III.A.2. *Shock-cell length prediction for BBSAN modeling*

The flight effects on the shock-cell length are studied in two separate paragraphs. Here, the length of the shock cells relevant for BBSAN is considered. The notched nozzle is used.

The positions of the shock-cell ends have been deduced from the schlieren pictures shown in figure 7 and they are displayed in figure 8. The first shock cells are seen to approximately have the same length between the three jets. In each case, the individual cell length decreases when moving downstream, which

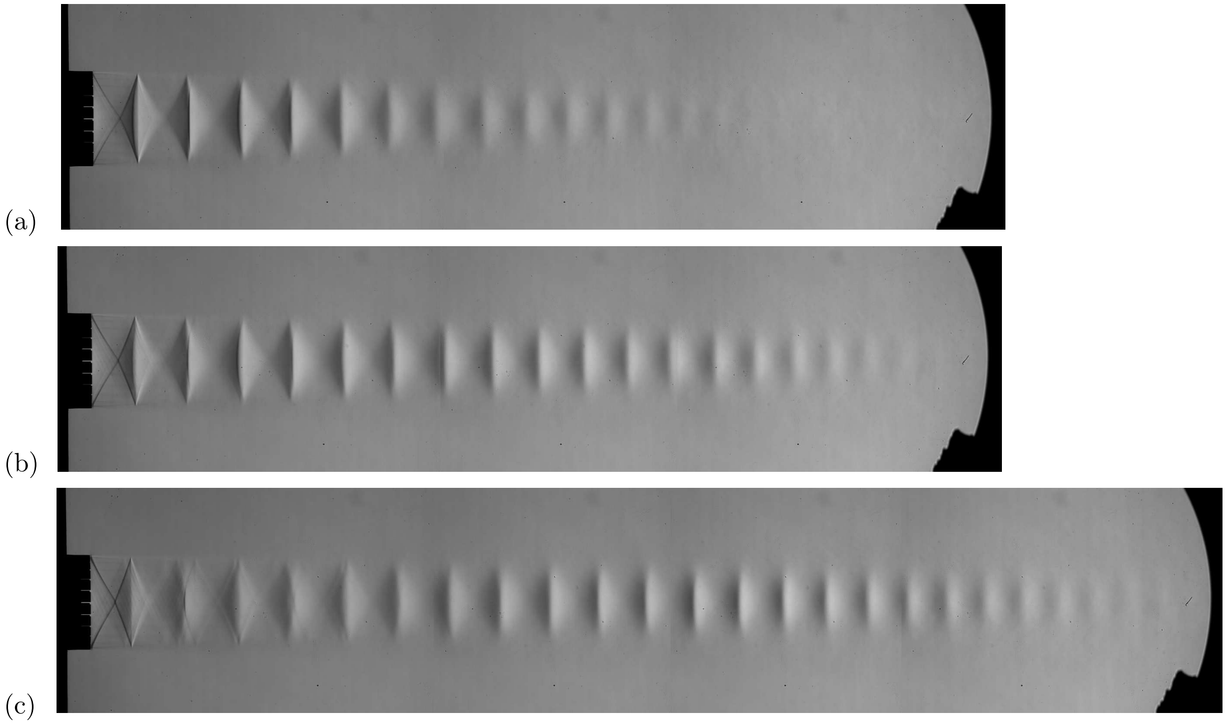

Figure 7. Mean schlieren images of three jets at $M_j = 1.10$ (notched nozzle). (a) $M_f = 0$, (b) $M_f = 0.22$, (c) $M_f = 0.39$. The pictures are made up of several images recorded at different axial locations.

is a typical feature of shock-cell patterns (refer to[10] for instance). This decrease is approximately linear, and straight lines have been fitted to each dataset. For $M_f = 0.39$, the two first cells are left out of the fit, because they are notably shorter. The slopes are −0.036, −0.028 and −0.026 βD per cell for $M_f = 0$, 0.22 and 0.39, respectively. Hence, the decrease in cell length is slowed down with secondary flow, which reflects the well-known shock-cell lengthening in flight.[12,16,33–35] It seems however incorrect to state, as it has been done before, that only the downstream shock cells are affected by flight : from figure 8, it is visible that the lengthening is continuous over the entire pattern.

The shock-cell lengthening is the product of several factors. The extension of the Prandtl-Pack vortex-sheet model[36,37] by Morris[33] shows that the cell lengthening is already a result of the modified boundary conditions existing near the exit of the supersonic jet. Furthermore, the more detailed analysis proposed by Michalke[35] demonstrates that for a finite shear layer thickness, the cell length is reduced when the thickness is increased. Thus, the thinner shear layer induced by flight (see section III..2) also entails a shock-cell lengthening.

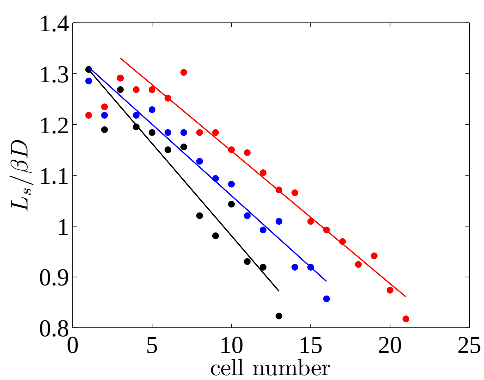

Figure 8. Length L_s of the individual shock cells non-dimensioned by βD, as obtained from the schlieren images presented in figure 7 ($M_j = 1.10$). • $M_f = 0$, • $M_f = 0.22$, • $M_f = 0.39$. The straight lines denote linear fits, whose slopes are -0.036, -0.028 and -0.026 βD per cell for M_f increasing.

The measurements shown in figure 8 could be used to express an empirical relation of the shock-cell lengthening induced by flight, which would be of interest for BBSAN modeling. Such a formula has been proposed by Tam[34] in the extension of his BBSAN theory to flight. It reads

$$\overline{L_s^{\mathrm{f}}} = \overline{L_s^{\mathrm{g}}}\,(1 + 0.625\,M_f) \tag{5}$$

where L_s^{f} and L_s^{g} are the mean shock-cell lengths in flight and on the ground ($M_f = 0$), respectively. In the current state of knowledge however, it does not seem possible to know which shock cells have to be considered to compute the mean. Indeed, it is still unclear which cells are responsible for BBSAN emission. It is believed that the downstream ones are more important in that respect,[38,39] but considering the significant lengthening of the shock-cell pattern, this approximate location is not precise enough for high values of M_f. Depending on which part of the pattern is chosen, the mean shock-cell length can quite vary. A more precise knowledge on BBSAN source location, in particular under flight conditions, is needed to conclude on a mean shock-cell length evolution from figure 8.

III.A.3. *Shock-cell length prediction for screech modeling*

A mean length of the cells responsible for screech is now calculated. It is known that screech is emitted by the first shock cells,[40,41] and the size of the second to fifth cells are averaged here, for each value of M_f (this assumes that the screech source does not slide downstream in flight). The results are shown in figure 9, obtained with the plain nozzle. The predictions of the vortex-sheet model by Morris[33] are included, as well as that of Tam's empirical formula (5). The shock spacing at $M_f = 0$ predicted by these models are matched with the measured data to compare only the flight-induced lengthening. When they match our conditions, data of Norum & Shearin[16] are also shown; they represent the mean length calculated on the same shock-cell interval. The present data have been obtained from pressure traverses and schlieren visualizations. This allows an uncertainty on the mean length to be estimated.

The mean length deduced from[16] is smaller than the one here, as well as its increase with M_f. Moreover, no model delivers a good comparison with the experimental values. This is not very surprising. Indeed, Morris' vortex-sheet model[33] should be valid close to the nozzle exit, where the shear layer is very thin, while here, shock cells extending a few diameters downstream are considered. In addition, Tam's formula (5) has been designed for predicting the evolution in flight of the downstream shock-cell length responsible for BBSAN, while here, the first few cells are isolated. It can be noted that this explanation is coherent with the slope relations between the present data and the models. Using a linear formulation for the cell lengthening reading

$$\overline{L_s^{\mathrm{f}}} = \overline{L_s^{\mathrm{g}}}\,(1 + a\,M_f) \tag{6}$$

the values $a = 0.12$ and 0.22 are found from the present data for $M_j = 1.10$ and 1.15, respectively. Other measurements at $M_j = 1.35$ and 1.50, not presented here, show that a increases with M_j.

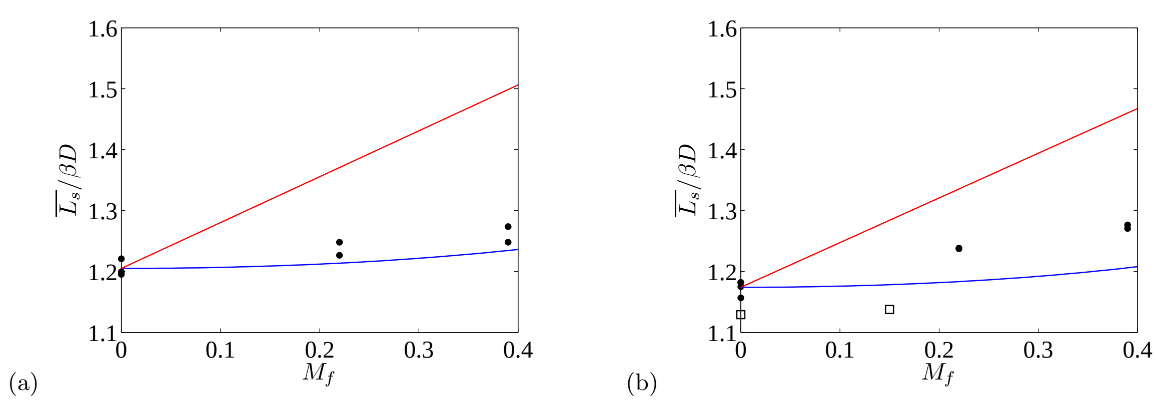

Figure 9. Mean shock-cell length for screech, non-dimensioned by βD and obtained by averaging the length of the second to fifth shock cells (plain nozzle). (a) $M_j = 1.10$, (b) $M_j = 1.15$. • Present data (from schlieren visualizations and pressure measurements), □ Norum & Shearin[16] ($\beta = 0.6$, or $M_j \approx 1.17$) ; —— Morris' model,[33] —— Tam's empirical expression (5).

III.A.4. Flight effects on the shock-cell strength

Static pressure profiles have been measured in jets exhausting from the plain nozzle. As discussed in reference,[20] screech induces a quicker damping of the shock-cell structure. However, the shock-cell strength should be approximately the same with and without screech for the cells existing in both jets. Furthermore, the results presented in the following are in full agreement with shock-cell strength estimates based on PIV data obtained with the screech-suppressing notched nozzle.

Only results for the jet centreline are shown. Off-axis measurements lead to the same conclusions as the ones established here.[42] The static pressure profiles have been acquired in two steps. A first coarse traverse has been performed, in order to localize the ends of the expansion (pressure minima) and compression regions (pressure maxima). Then, a second finer traverse is done, in which the measurement points are concentrated around the extrema of the coarse curve. So, the pressure extrema are better caught and the strength estimations are more accurate. Such finer profiles are presented in figure 10.

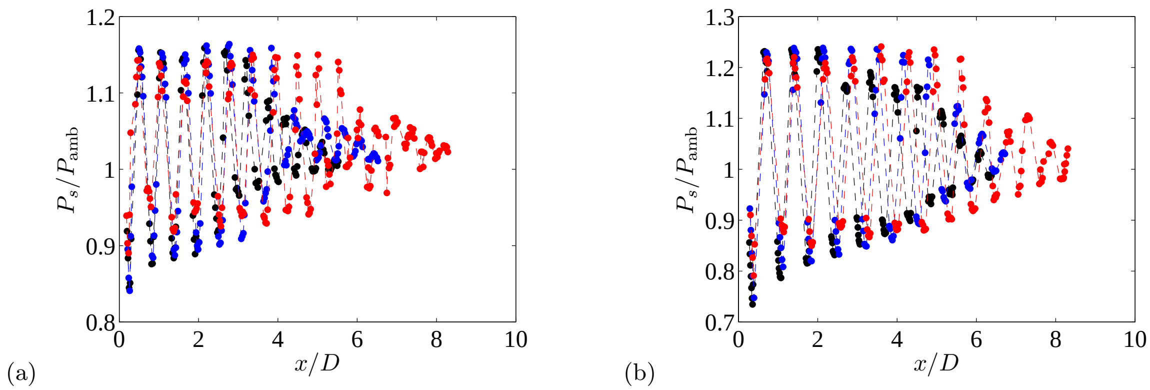

Figure 10. Centreline static pressure profiles, obtained with the plain nozzle; the measurement points are concentrated around the end of the expansion and compression regions in order to enhance the accuracy of the strength estimation. (a) $M_j = 1.10$, (b) $M_j = 1.15$. • $M_f = 0$, • $M_f = 0.22$, • $M_f = 0.39$.

The shock-cell strength can be expressed by $P_{\rm max}/P_{\rm min} - 1$,[43] with $P_{\rm max}$ ($P_{\rm min}$) the maximum (minimum) pressure in each cell. The strength calculated from the profiles displayed in figure 10 is presented in figure 11 for $M_j = 1.10$ and 1.15. Very consistent results are obtained for both jets. The small effect induced by a low flight speed is reminiscent of Norum & Shearin's results.[14] From $M_f = 0.22$ to 0.39, the pattern is markedly longer, which is associated with a decrease in the downstream attenuation rate of the cells. Furthermore, the first shock cells are weaker at $M_f = 0.39$.

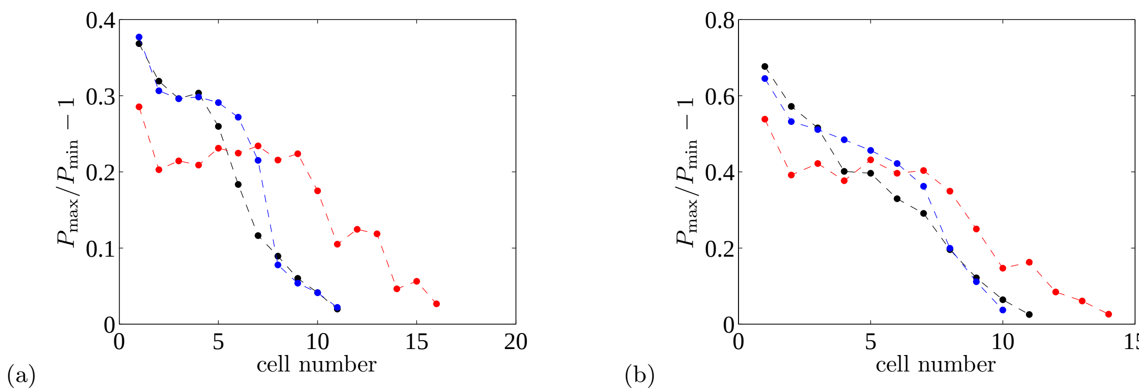

Figure 11. Shock-cell strength on the jet centreline, measured with the plain nozzle. (a) $M_j = 1.10$, (b) $M_j = 1.15$. • $M_f = 0$, • $M_f = 0.22$, • $M_f = 0.39$.

Usually, it is accepted that flight has no effect on the shock-cell strength.[16,34] However, a quantitative analysis of the data of Norum & Shearin[16] and Norum & Brown[17] shows that their results also present a decrease in the strength of the initial shock cells accompanied by an increase in the strength of the downstream cells.

III.A.5. Influence of the experimental conditions

The flight effect on the shock-cell strength observed here can be related, together with the effect on the shock-cell length, to the flight-induced lengthening of the entire pattern. The physical causes of the latter phenomenon are clear and they have been given in section III.A.1. However, all these influences of flight are not always as pronounced in other works as they are here. Some clues that can explain the discrepancies are discussed below.

Sarohia & Massier[25] showed the importance of the boundary layer thickness of the external flow for the flight effects on jet mixing noise (see also Drevet *et al.*[1] and the introduction of Michalke & Michel,[2]) and its influence was re-asserted by Sarohia[13] for the case of underexpanded jets. In the latter reference, it was shown in particular that the outer boundary layer thickness has an influence on the shock-cell length in flight. As mentioned above, Tam[34] considered that flight does not modify the strength of the shock-cell structure. He argued that the shock-cell pattern is determined by the pressure mismatch at the nozzle lip and that in a real flight configuration, the presence of a boundary layer on the outer side of the supersonic jet makes it very similar at this location to a case without external stream. It is thus believed that the flight effects on the shock-cell pattern will depend on the external boundary layer thickness, hence on the experimental set-up.

In the facility of Norum & Shearin[16] and Norum & Brown,[17] the primary jet exhausted 14 and 10 inches, respectively, downstream of the secondary stream exit plane. Here, both jets have the same exit plane. Hence, variations in the external boundary layer thickness are expected, which should also be affected by the geometry of the primary jet nozzle. Assuming that this boundary layer is thinner in the present experiment, it is expected that our results show a larger flight effect than those studies, in which the supersonic jet should be shielded on a larger distance by the outer boundary layer.

Another factor that can lead to discrepancies is the screech or probe noise that may appear during the static pressure measurements. Different levels of tonal noise during the acquisitions, be it screech or probe noise, can induce a disagreemment in the measured shock-cell structure. The abrupt damping of some patterns presented in Ref. 16 may be explained this way. Also, it might occur that the modal behavior of screech disrupts the measurements. Such a case can be seen in the figure 4 of Norum & Brown,[17] where a mode jump was responsible for the strong shortening of the cell pattern between $M_f = 0.3$ and 0.45.

IV. Conclusions

The flight effects on the turbulence properties and the shock-cell system of slightly underexpanded supersonic jets have been studied experimentally. Most of the results have been obtained with a screech-suppressing nozzle to better simulate the conditions arising in air transport.

The turbulence levels are constant in flight when the root-mean-square velocity fluctuations are non-dimensioned by the velocity difference between high-speed and low-speed flow. Because of the reduced mean shear across the mixing layer with external flow, its linear growth is slowed down when the flight Mach number M_f is increased. Accordingly, the growth of the turbulence length scales is slower in flight. The ratios of the growth rates of these length scales to the layer thickness show a consistent tendency to increase with flight velocity. This is believed to be a compressibility effect. Finally, an independence of the integral time scales in the convected frame on M_f has been found.

It has been observed that the shock-cell pattern is lengthened in flight, meaning that more shock cells are visible. This is due to the stretching of the entire flow coming from the reduced mixing layer growth rates. A concomitant effect is the lengthening of the individual shock cells. In particular, it has been shown that in a screech-suppressed jet, the length of the individual shock cells decreases approximately linearly with the cell number for all values of M_f, and that the rate of decrease is reduced when M_f is raised. While it appears difficult to deduce a mean shock-cell length for BBSAN modeling purposes, such a scale has been calculated for screech modeling in averaging the length of the initial cells of a screeching jet. A roughly linear variation of this mean shock spacing with M_f has been found, with a coefficient depending on the supersonic jet Mach number M_j. The evolution of the shock-cell strength has been obtained by detailed pressure measurements in a screeching jet. A small flight effect has been identified for $M_f = 0.22$, while the stretching of the shock-cell pattern was clearer at the highest M_f tested (0.39). It was accompanied by a decrease in the strength of the first shock cells.

The results on the extension of the shock-cell structure, and the related observations on the shock-cell strength, are in qualitative agreement with other measurements from the literature, although it is usually accepted that there is no flight effect on the strength of the cell structure. However, some tendencies obtained herein are not as pronounced in other studies. This can be linked to the appearance of screech or probe tones during the measurements, or also to the different external boundary layer thicknesses at the exit of the primary nozzle. It is indeed believed, as initially proposed by Sarohia,[13] that this boundary layer thickness has a non-negligible effect on the shock-cell structure in flight. It may also explain the fact that the turbulence levels, when defined the way presented in this paper, are here constant but not in other studies. In order to clearly demonstrate that this parameter is responsible for the discrepancies observed, it could be of interest to perform measurements with a varying external boundary layer thickness in a single facility.

Acknowledgments

The authors wish to thank Airbus Operations SAS (Mauro Porta) and Snecma (Guillaume Bodard) for their joint financial support, as well as Jean-Michel Perrin and Nathalie Grosjean for their help in setting up the experiment and the PIV measurement system.

References

[1] Drevet, P., Duponchel, J. P., and Jacques, J. R., "The effect of flight on jet noise as observed on the Bertin Aérotrain," *Journal of Sound and Vibration*, Vol. 54, No. 2, 1977.

[2] Michalke, A. and Michel, U., "Prediction of jet noise in flight from static tests," *Journal of Sound and Vibration*, Vol. 67, No. 3, 1979, pp. 341–367.

[3] Morris, P. J., "Turbulence measurements in subsonic and supersonic axisymmetric jets in a parallel stream," *AIAA Journal*, Vol. 14, No. 10, 1976, pp. 1468–1475.

[4] Tanna, H. K. and Morris, P. J., "In-flight simulation experiments on turbulent jet mixing noise," *Journal of Sound and Vibration*, Vol. 53, No. 3, 1977.

[5] Larson, R. S., McColgan, C. J., and Packman, A. B., "Jet noise source modification due to forward flight," *AIAA Journal*, Vol. 16, No. 3, 1978, pp. 225–232.

[6] Panda, J. and Seasholtz, R. G., "Measurement of shock structure and shock-vortex interaction in underexpanded jets using Rayleigh scattering," *Physics of Fluids*, Vol. 11, No. 12, 1999, pp. 3761–3777.

[7] André, B., Castelain, T., and Bailly, C., "Experimental exploration of underexpanded supersonic jets," *Accepted for publication by Shock Waves*, 2013.

[8] Powell, A., "On the mechanism of choked jet noise," *Proceedings of the Physical Society. Section B*, Vol. 66, No. 12, 1953, pp. 1039–1056.

[9] Raman, G., "Advances in understanding supersonic jet screech : Review and perspective," *Progress in Aerospace Sciences*, Vol. 34, No. 1-2, 1998, pp. 45–106.

[10] Harper-Bourne, M. and Fisher, M. J., "The noise from shock waves in supersonic jets," AGARD CP 131, 1973.

[11] Tam, C. K. W. and Tanna, H. K., "Shock associated noise of supersonic jets from convergent-divergent nozzles," *Journal of Sound and Vibration*, Vol. 81, No. 3, 1982, pp. 337–358.

[12] Bryce, W. D. and Pinker, R. A., "The noise from unheated supersonic jets in simulated flight," AIAA Paper 77-1327, 1977.

[13] Sarohia, V., "Some flight simulation experiments on jet noise from supersonic underexpanded flows," *AIAA Journal*, Vol. 16, No. 7, 1978, pp. 710–716.

[14] Norum, T. D. and Shearin, J. G., "Effects of simulated flight on the structure and noise of underexpanded jets," NASA Technical Paper 2308, 1984.

[15] Norum, T. D. and Shearin, J. G., "Shock noise from supersonic jets in simulated flight to Mach 0.4," AIAA Paper 86-1945, 1986.

[16] Norum, T. D. and Shearin, J. G., "Shock structure and noise of supersonic jets in simulated flight to Mach 0.4," NASA Technical Paper 2785, 1988.

[17] Norum, T. D. and Brown, M. C., "Simulated high speed flight effects on supersonic jet noise," AIAA Paper 93-4388, 1993.

[18] Rask, O., Kastner, J., and Gutmark, E., "Understanding how chevrons modify noise in a supersonic jet with flight effects," *AIAA Journal*, Vol. 49, No. 8, 2011, pp. 1569–1576.

[19] André, B., Castelain, T., and Bailly, C., "Experimental study of flight effects on screech in underexpanded jets," *Physics of Fluids*, Vol. 23, 2011, pp. 1–14.

[20] André, B., Castelain, T., and Bailly, C., "Broadband shock-associated noise in screeching and non-screeching underexpanded supersonic jets," *AIAA Journal*, Vol. 51, No. 3, 2013, pp. 665–673.

[21] Pinckney, S. Z., "A short static-pressure probe design for supersonic flow," NASA Technical Note D - 7978, 1975.

[22] Norum, T. D. and Seiner, J. M., "Measurements of mean static pressure and far field acoustics of shock containing supersonic jets," NASA Technical Memorandum 84521, 1982.

[23] André, B., Castelain, T., and Bailly, C., "Investigation of the mixing layer of underexpanded supersonic jets by particle image velocimetry," *Eigth International Symposium on Turbulence and Shear Flow Phenomena (TSFP-8)*, 2013.

[24] Goebel, S. G. and Dutton, J. C., "Experimental study of compressible turbulent mixing layers," *AIAA Journal*, Vol. 29, No. 4, 1991, pp. 538–546.

[25]Sarohia, V. and Massier, P. F., "Effects of external boundary-layer flow on jet noise in fight," *AIAA Journal*, Vol. 15, No. 5, 1977, pp. 659–664.

[26]Troutt, T. R. and McLaughlin, D. K., "Experiments on the flow and acoustic properties of a moderate-Reynolds-number supersonic jet," *Journal of Fluid Mechanics*, Vol. 116, 1982.

[27]Sarohia, V., "Flight effects on subsonic jet noise," AIAA Paper 79-616, 1979.

[28]Brown, G. L. and Roshko, A., "On density effects and large structure in turbulent mixing layers," *Journal of Fluid Mechanics*, Vol. 64, No. 4, 1974.

[29]Papamoschou, D. and Roshko, A., "The compressible turbulent shear layer: an experimental study," *Journal of Fluid Mechanics*, Vol. 197, 1988, pp. 453–477.

[30]Zaman, K. B. M. Q., "Asymptotic spreading rate of initially compressible jets - experiment and analysis," *Physics of Fluids*, Vol. 10, No. 10, 1998, pp. 2652–2660.

[31]Tam, C. K. W., "Stochastic model theory of broadband shock-associated noise from supersonic jets," *Journal of Sound and Vibration*, Vol. 116, No. 2, 1987, pp. 265–302.

[32]Fleury, V., Bailly, C., Jondeau, E., Michard, M., and Juvé, D., "Space-time correlations in two subsonic jets using dual particle image velocimetry measurements," *AIAA Journal*, Vol. 46, No. 10, 2008, pp. 2498–2509.

[33]Morris, P. J., "A note on the effect of forward flight on shock spacing in circular jets," *Journal of Sound and Vibration*, Vol. 121, No. 1, 1988, pp. 175–177.

[34]Tam, C. K. W., "Broadband shock-associated noise from supersonic jets in flight," *Journal of Sound and Vibration*, Vol. 151, No. 1, 1991, pp. 131–147.

[35]Michalke, A., "On the effect of external flow and shear-layer thickness on the expansion cells of under-expanded supersonic circular jets," *European Journal of Mechanics, B/fluids*, Vol. 11, No. 3, 1992, pp. 363–381.

[36]Prandtl, L., "Über die stationären Wellen in einem Gasstrahl," *Physikalische Zeitschrift*, Vol. 5, No. 19, 1904, pp. 599–601.

[37]Pack, D. C., "A note on Prandtl's formula for the wave-length of a supersonic gas jet," *The Quarterly Journal of Mechanics and Applied Mathematics*, Vol. 3, No. 2, 1950, pp. 173–181.

[38]Norum, T. D. and Seiner, J. M., "Broadband shock noise from supersonic jets," *AIAA Journal*, Vol. 20, No. 1, 1982, pp. 68–73.

[39]Seiner, J. M. and Yu, J. C., "Acoustic near-field properties associated with broadband shock noise," *AIAA Journal*, Vol. 22, No. 9, 1984, pp. 1207–1215.

[40]Lee, B. H. K. and Westley, R., "Effective axial source distribution in a choked screech jet," AIAA Paper 72-159, 1972.

[41]Umeda, Y. and Ishii, R., "On the sound sources of screech tones radiated from choked circular jets," *The Journal of the Acoustical Society of America*, Vol. 110, No. 4, 2001.

[42]André, B., *Etude expérimentale de l'effet du vol sur le bruit de choc de jets supersoniques sous-détendus*, Ph.D. Thesis, Ecole Centrale de Lyon, 2012.

[43]Seiner, J. M. and Norum, T. D., "Aerodynamic aspects of shock containing jet plumes," AIAA Paper 80-0965, 1980.